

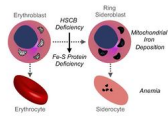
## Mutations in the iron-sulfur cluster biogenesis protein HSCB cause congenital sideroblastic anemia

Andrew Crispin, ... , Mark D. Fleming, Sarah Ducamp

*J Clin Invest.* 2020. <https://doi.org/10.1172/JCI135479>.

**Research** In-Press Preview **Genetics** **Hematology**

### Graphical abstract



**Find the latest version:**

<https://jci.me/135479/pdf>



***Mutations in the iron-sulfur cluster biogenesis protein HSCB cause congenital sideroblastic anemia***

**Authors and affiliations**

Andrew Crispin<sup>1</sup>, Chaoshe Guo<sup>1</sup>, Caiyong Chen<sup>2</sup>, Dean R. Campagna<sup>1</sup>, Paul J. Schmidt<sup>1</sup>, Daniel Lichtenstein<sup>1</sup>, Chang Cao<sup>1</sup>, Anoop K. Sendamarai<sup>1</sup>, Gordon J. Hildick-Smith<sup>2</sup>, Nicholas C. Huston<sup>2</sup>, Jeanne Boudreaux<sup>3</sup>, Sylvia S. Bottomley<sup>4</sup>, Matthew M. Heeney<sup>5</sup>, Barry H. Paw<sup>2</sup>, Mark D. Fleming<sup>1,6</sup>, Sarah Ducamp<sup>1,6</sup>

1 - Department of Pathology, Boston Children's Hospital, Boston, MA, 02115

2 - Division of Hematology, Brigham and Women's Hospital, Boston, MA, 02115

3 - Aflac Cancer and Blood Disorders Center, Children's Healthcare of Atlanta and Department of Pediatrics, Emory University, Atlanta, GA, 30322

4 - Department of Medicine, University of Oklahoma College of Medicine, Oklahoma City, OK, 73104

5 - Dana-Farber/Boston Children's Cancer and Blood Disorders Center, Boston, MA, 02115

6 – Corresponding authors

**Corresponding authors:**

Mark D. Fleming, MD, DPhil  
Department of Pathology  
Bader 139.1  
Boston Children's Hospital  
300 Longwood Avenue  
Boston, MA 02115  
[mark.fleming@childrens.harvard.edu](mailto:mark.fleming@childrens.harvard.edu)  
617-919-2664

Sarah Ducamp, PhD  
Department of Pathology  
Enders 1104  
Boston Children's Hospital  
300 Longwood Avenue  
Boston, MA 02115  
[sarah.ducamp@childrens.harvard.edu](mailto:sarah.ducamp@childrens.harvard.edu)  
617-355-3179

**Keywords:** HSCB, HSC20, sideroblastic anemia, iron-sulfur cluster

**Conflict of interest statement**

*The authors have declared that no conflict of interest exists.*

## Abstract

The congenital sideroblastic anemias (CSAs) can be caused by primary defects in mitochondrial iron-sulfur cluster (Fe-S) biogenesis. *HSCB* (heat shock cognate B), which encodes a mitochondrial co-chaperone, also known as *HSC20* (heat shock cognate protein 20), is the partner of mitochondrial heat shock protein A9 (HSPA9). Together with glutaredoxin 5 (GLRX5), HSCB and HSPA9 facilitate the transfer of nascent two-iron, two-sulfur ([2Fe-2S]) clusters to recipient mitochondrial proteins. Mutations in both HSPA9 and GLRX5 have previously been associated with CSA. Therefore, we hypothesized that mutations in *HSCB* could also cause CSA. We screened patients with genetically undefined CSA and identified a frameshift mutation and a rare promoter variant in *HSCB* in a female patient with non-syndromic CSA. We found that HSCB expression was decreased in patient-derived fibroblasts and K562 erythroleukemia cells engineered to have the patient-specific promoter variant. Furthermore, gene knockdown and deletion experiments performed in K562 cells, zebrafish, and mice demonstrate that loss of HSCB results in impaired Fe-S cluster biogenesis, a defect in red blood cell hemoglobinization, the development of siderocytes, and more broadly perturbs hematopoiesis *in vivo*. These results further affirm the involvement of Fe-S biogenesis in erythropoiesis and hematopoiesis and define *HSCB* as a CSA gene.

## Introduction

The Congenital Sideroblastic Anemias (CSAs) are a group of uncommon inherited blood disorders characterized by abnormal iron accumulation in the mitochondria of erythroid cells. As the normal location of erythroid mitochondria is in the vicinity of the nucleus, the pathological iron deposits appear to ring the nucleus, resulting in the characteristic “ring sideroblast.” The mitochondrion is the nexus of iron metabolism in the erythroid progenitor, being the site of iron incorporation into protoporphyrin IX to form heme, and essential for iron-sulfur (Fe-S) cluster biogenesis. Genes in multiple pathways contribute to the pathogenesis of CSA, including those involved in heme biosynthesis (*ALAS2*, *SLC25A38*), mitochondrial Fe-S cluster assembly and transport (*ABCB7*, *GLRX5*, *HSPA9*), mitochondrial protein synthesis (mt-DNA deletions, *TRNT1*, *LARS2*, *YARS2*, *PUS1*), and mitochondrial energy metabolism (mt-DNA deletions, *MT-ATP6*, *SLC19A2*, *NDUFB11*) (1). However, many cases of CSA remain genetically unexplained. The identification of the genetic defects responsible for CSA will assist in predicting clinical comorbidities and may guide the design of subtype-specific therapies, which are, unfortunately, limited at this time. More fundamentally, the mechanisms leading to the formation of the ring sideroblast and the physiopathology underlying these diseases are still not well understood.

Of the CSAs, those due to mitochondrial Fe-S cluster assembly defects are the rarest. Only five families have been reported with mutations in the ATP binding cassette transporter subfamily B member 7 (*ABCB7*), three with glutaredoxin 5 (*GLRX5*) mutations, and 11 with heat shock protein family A member 9 (*HSPA9*, also known as mortalin) mutations (1). The mitochondrial Fe-S pathway can be subdivided into 3 steps: *de novo* assembly of the Fe-S on a scaffold protein, release of the nascent cluster, and transfer and insertion of the cluster into target apoproteins (For review, 2, 3). *ABCB7* is a putative mitochondrial “Fe-S cluster exporter” involved in cytosolic Fe-S cluster protein maturation; *HSPA9* and *GLRX5* are involved in the scaffold release step. *HSPA9* encodes a mitochondrial chaperone belonging to the HSP70 family of heat shock

proteins. The essential cochaperone of HSPA9, HSCB (heat shock cognate B, also known as HSC20), stimulates the ATPase activity of HSPA9 and facilitates the release of the newly formed [2Fe-2S] from the scaffold protein, ISCU (Iron-Sulfur Cluster Assembly Enzyme), and transfers it to GLRX5. GLRX5 is the immediate donor of [2Fe-2S] clusters to target apoproteins as well as to subsequent assembly factors that convert the [2Fe-2S] cluster to a [4Fe-4S] cluster. One of the mitochondrial recipient proteins is ferrochelatase (FECH), the last enzyme in heme biosynthesis, which is a dimer stabilized by two [2Fe-2S] clusters that are essential for its activity (4). Other targets include respiratory complexes I, II and III, which incorporate structural and catalytic [2Fe-2S] and [4Fe-4S] clusters required for the electron transport chain. Disruption of mitochondrial Fe-S assembly also impairs the maturation of cytosolic Fe-S proteins, including the bifunctional protein IRP1/ACO1 (iron regulatory protein 1/cytosolic aconitase). IRP1 and its functional ortholog, IRP2, control intracellular iron homeostasis by binding to mRNA stem-loops termed iron responsive elements (IREs), located in either the 5' or 3' untranslated regions (UTR) of genes relevant to iron metabolism, affecting mRNA translation or stability, respectively. In the setting of iron deficiency or cytosolic Fe-S deficiency, IRP1/ACO1 is an active IRP, favoring iron uptake and limiting its utilization. IRP2 is degraded in the presence of increased levels of cytosolic iron in an Fe-S cluster-dependent manner (5). Among those target mRNAs with 5'IREs that are repressed by iron or Fe-S deficiency is the erythroid isoform of  $\delta$ -aminolevulinate synthase (ALAS2), the first and rate limiting enzyme of heme biosynthesis. Thus, Fe-S biogenesis defects can influence multiple aspects of heme and mitochondrial respiratory protein function, all of which are implicated in CSA.

Given the requirement for HSCB in Fe-S cluster biogenesis, we hypothesized that HSCB mutations could cause CSA. Accordingly, we screened patients with genetically unexplained CSA, initially by targeted Sanger sequencing and subsequently by whole exome sequencing (WES), for rare HSCB variants. We identified one proband with biallelic variants: a frameshift

variant, Thr87Asnfs\*27, and an ETS transcription factor binding site variant in the promoter region. We established that the variants segregated with the disease in the family and that HSCB expression was reduced in the patient's skin fibroblasts. We conducted experiments that validated the pathogenicity of the variants, including the effect of the promoter allele on HSCB expression. We also studied the impact of HSCB loss on erythropoiesis and hematopoiesis in cell culture and *in vivo* models, demonstrating its effect on Fe-S-dependent enzymes, oxidative phosphorylation, iron metabolism and hemoglobinization in an erythroid context, including the evolution of siderocytes in a mouse model, affirming the causative nature of the mutations in this patient.

## Results

### Biallelic loss of function *HSCB* variants in a patient with CSA.

We evaluated 141 probands with CSA for *HSCB* mutations by Sanger sequencing and/or WES. Mutations in known CSA genes were subsequently identified in 71 of these patients by candidate gene sequencing or WES (data not shown). Three of the 141 patients carried rare (minor allele frequency [MAF] <0.005) variants in *HSCB*. In two of them, their CSA could be accounted for by mutations in other genes (*ALAS2* and *PUS1*). One female patient (Figure 1A) carried a frameshift variant (NM\_172002.4, c.259dup; p.Thr87Asnfs\*27) not present in the gnomAD database (<http://gnomad.broadinstitute.org/>) as well as a rare promoter variant (c.-134G>A; rs551244874, gnomAD MAF  $9.69 \times 10^{-5}$ ). The overall loss of function (LOF) allele frequency for *HSCB* is  $7.66 \times 10^{-6}$  in gnomAD with no reported homozygotes for any LOF allele, suggesting that null-individuals are not viable. The *HSCB* variants segregate with the disease in the family and are present in the patient's fibroblasts, confirming that neither variant is somatic (Figures 1C & 1D). WES of the patient, her brother, and parents revealed no mutations in other genes known to be associated with CSA.

The proband was discovered to be anemic at the age of 10. At age 13, she was diagnosed with a suprasellar germ cell tumor that was treated with craniospinal radiation (Table 1). Because of persistent anemia and evolving pancytopenia, a bone marrow aspiration and biopsy were performed at age 15 years. Iron staining of the aspirate revealed ring sideroblasts (Figure 1B). She has been chronically transfused since the age of 17. At age 20 years, at the time of this study, she had mild neutropenia and moderate thrombocytopenia. Now age 26 years, she is clinically stable. Given the history of radiation therapy, we compared patient's peripheral blood and skin fibroblasts exome sequences and found no somatic variants indicative of a myelodysplastic syndrome (MDS), including those associated with acquired sideroblastic anemia (e.g., *SF3B1*

mutations, data not shown). Furthermore, X-inactivation studies performed on peripheral blood demonstrated that the patient's hematopoiesis was not clonal (data not shown).

The mRNA transcribed from the *HSCB* coding sequence variant, p.Thr87Asnfs\*27, is likely degraded by nonsense mediated decay, and/or to encode a prematurely truncated, non-functional protein lacking the DNA-J domain, responsible for the interaction with HSPA9, and the C-terminal helix, critical for ISCU binding. We hypothesized that the promoter variant, which is located in a DNase hypersensitive site in human CD34<sup>+</sup> hematopoietic stem cells (Encode), adversely affects *HSCB* transcription. We used the Genomatix MatInspector software to determine potential transcription factor binding sites in the region of the variant (Figure 1E). *In silico*, the c.-134G>A variant is predicted to disrupt the core sequence of a binding site for an E26 Transformation-Specific (ETS) DNA binding factor. There are 28 human ETS transcription factors, each of which binds a conserved DNA motif (GGAA/T); surrounding sequences determine the binding specificity of different family members (6). To determine if the patient's variant alleles impaired *HSCB* expression, we measured *HSCB* protein levels by western blot (Figure 1F). *HSCB* protein expression in the proband's fibroblasts was ~75% (24±11% residual protein, t test P<0.001, Figure 1G) less than in two unrelated skin fibroblast controls. Homozygous c.-134G>A mutant K562 human erythroleukemic cell lines expressed less *HSCB* protein than their control counterparts (~85%, n=2 and n =4 G/G c.-134A/A and G/G clones, respectively, t test P=n.s.), suggesting the possibility of functional significance of this sequence variant (Figure 1H). We did not have access to CD34<sup>+</sup> hematopoietic precursor cells from the proband, limiting our ability to evaluate the effect of the patient's mutations on chromatin binding and/or gene expression and cellular phenotypes in primary erythroid cells. Consequently, to further test our hypothesis that the ETS binding site variant is responsible is the second, recessive allele, we performed chromatin immunoprecipitation of ETS1, one of the primary hematopoietically expressed ETS factors, in K562 cells and found that ETS1 does indeed occupy the *HSCB* promoter region (Figure

1I). We also examined the activity of the HSCB promoter c.-134G>A variant in a luciferase reporter assay in HeLa cells (Figure 1J). We found that expression of ETS1 produced a dose-dependent increase in luciferase activity in the WT c.-134G promoter construct that was attenuated in the c.-134A variant construct. Taken together, these results confirm that the *HSCB* sequence variants detected in the proband CSA patient collectively result in decreased HSCB protein expression.

### **Depletion of HSCB perturbs oxidative phosphorylation, iron metabolism and hemoglobinization in K562 erythroleukemia cells.**

Previous characterization of mammalian HSCB has been performed in non-hematopoietic, non-erythroid cells (7-9), but the regulation of iron homeostasis, heme biosynthesis and Fe-S cluster assembly are unique in erythroid cells. Moreover, germline defects in *GLRX5* and *HSPA9*, two other proteins that mediate Fe-S cluster transfer, largely affect erythropoiesis (1). To determine the effects of HSCB in an erythroid system, we performed shRNA knockdown experiments in undifferentiated and differentiated K562 erythroleukemia cells. HSCB depletion to levels similar to those in the patient's fibroblasts (Figures 2A-2D and Supplemental Figures 1A, 1B & 1C), did not affect *HSPA9* expression, but did reduce expression of mitochondrial enzymes containing Fe-S clusters, such as *FECH* and mitochondrial aconitase (*ACO2*), as well as multiple respiratory complex (RC) proteins containing Fe-S cluster-dependent subunits. HSCB knockdown also impaired the lipoylation of the E2 subunits of the pyruvate and  $\alpha$ -ketoglutarate dehydrogenase complexes likely because lipoic acid biosynthesis requires an Fe-S enzyme (10). Commensurate with the reduction of tricarboxylic acid cycle (TCA) enzymes and RC proteins, Seahorse extracellular flux analysis showed that HSCB depleted K562 cells are less energetic, are more dependent on glycolysis, and have reduced oxidative phosphorylation capacity (Figures 2E-2G). These results are concordant with those previously observed in HeLa cells (8).

We also investigated iron metabolism in *HSCB*-shRNA treated cells. Interestingly, IRP protein expression was slightly decreased in erythroid *HSCB* depleted cells (Figure 3A). This result was unexpected, as previous work had demonstrated increased IRP1 activity, but unaffected protein levels (9). Despite the reduced IRP1 and IRP2 protein levels, expression of IRP target proteins was consistent with increased IRP activity; both ferritin L and H chain expression were decreased, whereas cell surface TFR1 expression was increased (Figures 3A, 3B, and 3E). We also determined that *HSCB*-depleted cells were able to respond to iron chelation and overload. We found that reduced expression of *HSCB* results in retained, but attenuated responses (Figures 3C, 3D, & 3F).

To evaluate erythroid-specific phenotypes in the context of *HSCB* depletion, we repeated the analyses in K562 cells induced to differentiate by exposure to sodium butyrate for 96 hours. We found that depletion of *HSCB* impaired expression of ferrochelatase and fetal hemoglobin, the major hemoglobin expressed by K562 cells (Figures 3G-3J, Supplemental Figures 1D & 1E). These findings are consistent with reduced *HSCB* levels being responsible for the hypochromic microcytic anemia observed in the patient.

**Knockdown of zebrafish *hscb* demonstrates an erythropoietic defect that is partially rescued by IRE-less *alas2*.**

To further assess the role of *HSCB* in erythropoiesis, we examined *hscb* mRNA expression and the effect of *hscb* knockdown in zebrafish embryos. We found that *hscb* is expressed throughout the embryo and not disproportionately expressed in hematopoietic tissues (Figure 4A). However, morpholino knockdown of *hscb* resulted in an embryo with a grossly normal body plan, but a reduced number of erythrocytes and decreased hemoglobinization (Figures 4B & 4C and Supplemental Figures 2A & 2B). Similar to *HSCB*-knockdown K562 cells, expression of the erythroid-specific form of the transferrin receptor was upregulated in *hscb* morphant embryos,

suggesting activation of IRPs (Supplemental Figure 2C). IRE-dependent suppression of ALAS2 translation likely contributes to the pathogenesis of Fe-S cluster deficiency related CSAs (11). To determine if this is also the case in HSCB deficiency, we co-injected *hscb* zebrafish embryo morphants with mRNAs encoding wild-type zebrafish *alas2*, wild type *alas2* with a mutated 5'IRE, and *alas2* with a premature stop codon also lacking the 5'IRE. We found that only the IRE-less *alas2* mRNA encoding the wild type protein partially rescued the phenotype (Figure 4C), indicating that some of the HSCB deficiency erythroid phenotype can be attributed to an *alas2*-5'IRE-dependent mechanism.

***Hscb* is an essential gene in mice and its loss in hematopoietic tissues results in siderocytic anemia and loss of hematopoietic progenitors.**

To examine the effect of HSCB deficiency in an intact mammal, we created null and conditionally targeted mouse *Hscb* alleles. Homozygous *Hscb* null (*Hscb*<sup>-/-</sup>) embryos were not observed as early as embryonic day 7.5 (E7.5), indicating that germline *Hscb* deficiency is lethal in early embryogenesis. To determine the effect of *Hscb* loss on erythropoiesis, we bred the conditionally targeted allele (*Hscb*<sup>fl/fl</sup>) to a transgenic line expressing Cre recombinase under the control of the erythropoietin receptor (*Epor*<sup>tm1(EGFP/cre)UK</sup>, *Epor-Cre*), that is restricted to erythroblasts beginning at E10.5 (12). *Hscb*<sup>fl/fl</sup> *Epor-Cre*<sup>+</sup> animals uniformly died of anemia prior to E14.5 (Figure 5A). A subset of circulating nucleated erythrocytes contained coarse iron granules, typical of those seen in sideroblastic anemia, were observed only in *Hscb*<sup>fl/fl</sup> *Epor-Cre*<sup>+</sup> embryos at E11.5 (Figure 5B).

By contrast, *Hscb*<sup>fl/fl</sup> animals carrying a *Vav1-Cre* transgene that leads to pan-hematopoietic deletion, yielded grossly normal live-born mice in the expected Mendelian ratio. However, soon after birth, these animals began to exhibit growth delay and became pale (Figure 6A); most died of bacterial pneumonia between post-natal days 4 and 7 (P4-P7, Supplemental Figure 3). *Hscb*<sup>fl/fl</sup> *Vav1-Cre*<sup>+</sup> P7 pups had atrophic spleens, pale coloration of bones (Figure 6B), and extremely

limited hematopoiesis in the bone marrow, liver, and spleen (Figure 6C, Supplemental Figure 3C & 3D). *Hscb<sup>fl/-</sup> Vav1-Cre<sup>+</sup>* were profoundly pancytopenic, with decreases in the RBC, white blood cell and platelet counts (Figures 6D-6F). The hemoglobin and hematocrit were markedly decreased, whereas the mean cellular volume (MCV) was normal (data not shown). Terminal and stress erythropoiesis were assessed in marrow and spleen by flow cytometry (13). Ter119/CD44 staining showed a near complete absence of early and late stage erythroblasts in the marrow (Figure 6G) and spleen (data not shown) of knockout animals, demonstrating that Hscb is required for murine normal and stress erythropoiesis.

To further evaluate the role of Hscb in murine hematopoiesis, we transplanted lethally irradiated, congenic adult wild type recipient mice with E14.5 fetal liver hematopoietic stem cells from *Hscb<sup>fl/-</sup>* animals with or without an inducible *Mx1-Cre* transgene. We allowed the chimeras to engraft for 8 weeks, after which, Cre recombinase was induced by poly-inosine, poly-cytosine (pIpC) injections on alternate days for 5 days (3 doses), and quantitative and qualitative hematologic parameters followed for three weeks (Supplemental Figure 4A). No quantitative differences were observed in the first week, however, beginning on day 5, and peaking on day 7, a transient population of siderocytes appeared in the peripheral blood of the recipients transplanted with *Hscb<sup>fl/-</sup> Mx1-Cre<sup>+</sup>* hematopoietic stem cells (Figures 7A & 7B). Thereafter, steep drops in the red blood cell count, hemoglobin, white blood cell count, and platelet count necessitated euthanasia of most mice by day 22 (Figures 7C, 7D, 7E, & 7F, Supplemental Figures 4B & 4C). Histologically, the bone marrow was nearly acellular, lacking any recognizable hematopoietic elements (data not shown). Flow cytometry analysis supported the absence of erythroid progenitors in the bone marrow (Figure 6G) and spleen (data not shown), confirming that steady-state and stress erythropoiesis are both affected by Hscb depletion.

## Discussion

Here, in a very large cohort of patients with CSA, we identify an individual with two variants in the mitochondrial heat shock protein co-chaperone HSCB. We demonstrate using patient-derived and induced-mutant cell lines that each variant decreases protein expression and that loss of HSCB reduces Fe-S cluster protein abundance, cellular respiration, and erythroid differentiation. Furthermore, studies in zebrafish *hscb*-morphant embryos and genetically engineered, *Hscb*-deficient mice indicate that HSCB is particularly important for erythropoiesis and can induce the accumulation of erythroid iron. *In toto*, this provides strong evidence that these mutations are causative of the sideroblastic phenotype in this patient. This result is congruent with the fact that mutations in other proteins, including HSPA9—HSCB's chaperone partner—and the mitochondrial glutaredoxin, GLRX5, and ABCB7, involved in the transfer of nascent Fe-S clusters to recipient mitochondrial and cytosolic proteins, result in a CSA phenotype. As such, it further solidifies the understanding of this class of disorders.

Furthermore, we also noted that the patient developed moderate thrombocytopenia and leukopenia over time (Table 1). In this regard, we observed that complete *Hscb* loss leads to not only anemia, but also bone marrow failure in mouse models. Flow cytometry experiments performed using bone marrow from both *Vav1-Cre*<sup>+</sup> (Supplemental Figure 5) and *Mx1-Cre*<sup>+</sup> (not shown) animals demonstrated that lineage positive (*Lin*<sup>+</sup>) cells were dramatically decreased. Nonetheless, lineage negative, *Sca1*<sup>+</sup>, *Kit*<sup>+</sup> (*Lin*<sup>-</sup>*Sca1*<sup>+</sup>*Kit*<sup>+</sup>) cell population persisted. It is unclear if this result reflects the ability of these cells to persist in the absence of *Hscb*, or an effect related to the onset of *Cre* transgene expression.

The apparent rarity of the HSCB, and indeed the HSPA9 and GLRX5, related anemias and their cell type selectivity may be a consequence of both the essential nature of HSCB in mammalian cells and a unique sensitivity or dependence of this pathway in erythroblasts. The early embryonic

lethality of *Hscb* null mouse embryos demonstrated here and the severe, respiratory-deficient phenotypes seen in yeast loss-of-function mutants (14) argue that a human null in any of these genes would be inviable. In the HSPA9 anemia, which is the most commonly described of Fe-S associated CSAs, a variety of null alleles are present in trans of a functionally mild missense variant or a common variant (minor allele frequency of ~30-40%) at rs10117T, which is associated with reduced *HSPA9* mRNA expression (15). Indeed, the relative frequency of this common variant may account for the more frequent occurrence of the HSPA9 associated disease; any null allele occurring in the population stands a good chance to be in trans of this low-expresser variant, resulting in sufficient loss-of-function to cause a mild sideroblastic phenotype. Similarly, we provide evidence here that reduced protein expression caused by a mutation in an ETS transcription factor binding site in the promoter of *HSCB* results in reduced protein expression in K562 cells. It is possible that a deficiency of ETS factor binding at this site contributes to the erythroid and hematopoietic restriction of the patient's phenotype. Indeed, in contrast to fibroblasts from patients with *GLRX5* deficiency due to missense mutations (16), we observed no abnormalities of Fe-S cluster protein expression or respiratory function in *HSCB* patient-derived fibroblasts (data not shown), suggesting that the c.-134A>G allele has little overall effect on *HSCB* expression in fibroblasts, or that fibroblasts are more tolerant than erythroid cells to Fe-S cluster loss.

Save for ferrochelatase mutations, which result in erythropoietic protoporphyria and an equivocal sideroblastic phenotype (17), it is unclear why mutations in specific Fe-S cluster recipient proteins or in proteins involved in earlier steps in Fe-S cluster biogenesis do not result in CSA. In particular, defects in the initial assembly of the Fe-S cluster tend to result in complex neuro-metabolic phenotypes. It may be that Fe-S clusters or their precursors are particularly toxic or accumulate in the iron- and heme-rich environment of the erythroblast mitochondrion. Alternatively, given the impact of Fe-S cluster deficiency on heme synthesis—mediated by both ferrochelatase deficiency

and, through the hyperactivation of IRP1, IRE binding activity and concomitant ALAS2 down-regulation—there may be insufficient heme at critical stages of erythroid maturation to sustain a heme-dependent network of differentiation and survival signals (18, 19). Heme deficiency is likely in part contributory, as this and other work has consistently shown that rendering *ALAS2* expression IRE-independent has a salutary effect on Fe-S cluster-deficient erythropoiesis (11). Such a strategy could, in theory, be exploited therapeutically.

In conclusion, our work establishes *HSCB* as a new mitochondrial Fe-S associated CSA gene. Moreover, we confirm the aberrant activity of IRPs in this context and demonstrate that targeting the *alas2-IRE*, and releasing the repressive effect of IRPs on translation, can be sufficient to prevent the anemia. Finally, we showed that *HSCB* is not required only for erythropoiesis and hemoglobinization but also more generally for hematopoiesis.

## Methods

**Study approval.** Written informed consent was obtained from all participants on Boston Children's Hospital (BCH) human subjects research protocol 06-12-053. Animal experiments were approved by the Animal Care and Use Committee at BCH.

**Sequencing.** Except as noted, DNA was prepared from peripheral blood using the PureGene DNA isolation kit (Gentra). For Sanger sequencing, the *HSCB* promoter region (c.-250 to c.-1), exons, and intron-exon junctions were amplified and sequenced using the primers described in Supplemental Table 1 and analyzed with Sequencher 5.4.1. Paired end whole exome sequencing (WES) libraries were prepared with the Agilent SureSelect V5 exon selection kit and sequenced to a median depth of ~100x with 100 bp paired end reads on an Illumina NextSeq2500 instrument. Data were processed on an internally validated pipeline and analyzed on the WuXi NextCODE genomics platform ([www.wuxinextcode.com](http://www.wuxinextcode.com)).

**Cell culture.** Primary fibroblasts and HeLa cells were cultured in Dulbecco's Modified Eagle Medium (DMEM, 11965-092, Gibco) and K562 cells in RPMI 1640 medium (11875-093, Gibco). All media were supplemented with 10% fetal bovine serum (FBS, Sigma-Aldrich), 2 mM glutamine (Corning) and 100 IU/mL Penicillin/100µg/mL Streptomycin (Corning) and described as "complete media." Primary fibroblasts were cultured from a skin biopsy from the proband or discarded skin samples from unrelated healthy females. Fibroblasts were passaged, frozen or harvested at ~80% confluence. For HSCB depletion experiments, K562 cells were infected with Mission Lentiviral Transduction particles encoding shRNA control (shSC: SHC002V) or shRNA directed against HSCB (Sigma-Aldrich; SHCLNV, TRCN000013- 4428, 4940, 8234 ("sh1"), 8487 ("sh2") and 8909) according to the manufacturer's instructions. Briefly 0.1M cells were combined with 7.5µL lentiviral particles. A non-infected (NI) well was employed as a control. At 24 hrs following infection, cells were diluted with complete media, and at 72 hrs cells were washed 3 times in sterile 1xPBS and resuspended in complete media supplemented with puromycin (1 µg/mL, Gibco

A11138-03) for infected cells. Experiments were conducted between day 6 and day 21. Control and HSCB-depleted K562 were treated with 0.6mM sodium butyrate (Sigma-Aldrich 30342) to induce hemoglobinization, 0.1 mM deferiprone (DFP, Sigma-Aldrich 379409) for iron chelation, and 200  $\mu$ M iron:nitrilotriacetic acid (FeNTA, ferric iron, Sigma-Aldrich F7134 and nitrilotriacetic acid, Sigma-Aldrich N9877) for iron overload.

**CRISPR-Cas9 gene editing.** K562 cells were edited by CRISPR-CAS9 technology according to established protocols (20). Briefly, a single guide RNA (sgRNA) adjacent to the promoter HSCB variant was selected using Deskgen software (<https://www.deskgen.com/landing/>) (g/AGAGCGGAACTTAGAACCC, where g is an additional nucleotide; activity score: 67; off-target score: 87). Annealed complementary sgRNAs annealing were cloned in pSpCas9(BB)-2A-GFP (PX458, Addgene) using BbSI restriction enzyme and T4 ligase (New England Biolabs) and clones sequence verified, propagated, and purified using PureLink™ HiPure Plasmid Filter Maxiprep Kit (ThermoFisher), quantified (Nanodrop), and resequenced. Two symmetric templates of reparation (ssODN) were designed and purchased (Integrated DNA Technologies): one to edit only the corresponding GGG- Protospacer Adjacent Motif (PAM) sequence

(CTCAATGCCTCCTGGGAGTTGTAGTTTAGAAGGGAGAGC

GGAACTTAGAACCCTTTTTCCCCTCGGGTGATCCCGCCCCCTCGACTCCCCAGCCAATCA

G, where G is the wild-type promoter variant and TTT the edited PAM; ssODN PAM) and the other one to edit the PAM site and the targeted locus

(CTCAATGCCTCCTGGGAGTTGTAGTTTAGAAGGGAGAGCAGAACTTAGAACCCTTTTTCC

CCTCGGGTGATCCCGCCCCCTCGACTCCCCAGCCAATCAG, where A is the mutated promoter variant; ssODN-MUT). Genomatix software was used to analyze the impact the of PAM

site editing and the TTT substitution was selected on the basis of the weakest impact predicted

*in silico*.  $1 \times 10^6$  K562 cells were nucleofected with 3  $\mu$ g PX458-HSCB and 30  $\mu$ M ssODNs (either the ssODN-PAM or ssODN-MUT) using an Amaxa Nucleofector 2b device (Lonza), the Cell Line

Nucleofector® Kit V, and program T-016 according to the manufacturer's instructions. After nucleofection, the cells were resuspended in 0.5 mL of complete RPMI and transferred to a 6 well plate filled with 1.5 mL of RPMI supplemented with 1  $\mu$ M SCR7, an inhibitor of DNA ligase IV and non-homologous end joining (Sigma-Aldrich). After 24 hrs, single GFP<sup>+</sup> cells were sorted using an ARIA III (BD Bioscience) in 96 well U-well plate filled with 200  $\mu$ L complete RPMI and expanded for 15 days. Wells containing single colonies were identified visually, DNA prepared with QuickExtract™ DNA Extraction Solution (Lucigen), and amplified with target specific primers, sequenced and analyzed with Sequencher 5.4.1. Two independent clones homozygous for the PAM modification only and two independent clones homozygous for the PAM modification and the promoter variant were identified, expanded, and re-sequenced after two weeks in culture.

**Western blotting.** Cells pellets were resuspended in Laemmli buffer 1X solution (62.5 mM Tris HCl pH 6.7, 10% Glycerol and 2% SDS final concentrations) and denatured for 5-10 min at 90°C. Protein content was quantified with the DC protein colorimetric assay (BIO-RAD) using serum albumin standards. For all K562 experiments, at least 3 independent infections were performed to obtain samples for immunoblotting. 15-40  $\mu$ g of total protein, supplemented with 40 mM DL-dithiothreitol (DTT, Sigma-Aldrich D9779) and bromophenol blue were loaded in TruPAGE, 4-20%, 4-8% or 12% pre-cast acrylamide gels (Sigma-Aldrich) and run with TruPAGE SDS running buffer (Sigma-Aldrich PCG3001). Transfers were performed on nitrocellulose membranes (Bio-Rad, 1620112) using transfer buffer (100 mM glycine, 17 mM Tris base, 20% ethanol), and the efficiency of transfer assessed by Ponceau Red staining. Membranes were cut according to the loaded ladder (Dual Color, Bio-Rad), and blocked at least one hour at room temperature (RT) with agitation in Tris-buffered saline buffer with 0.1% Tween 20 (TBS-t) supplemented with 5% nonfat-dry milk. Membranes were incubated overnight with primary antibodies (Supplemental Table 2) at 4°C with agitation. Membranes were washed 30 min with TBS-t and incubated with secondary antibodies conjugated with horseradish peroxidase (Supplemental Table 3) one hour, at RT with

agitation. Membranes were washed again, and detection was performed on a ChemiDoc MP analyzer using different sensitivity ECL detection reagents (Prime or Select, GE Healthcare) depending on the protein of interest. Membranes were stripped in TBS-t, reblotted with other primary antibodies or stored at -20°C for subsequent reuse. ECL images were captured electronically with Image Lab 5.2.1 (Bio-Rad) and protein expression quantitated by densitometry using Image Studio Lite (LI-COR Biosciences).

**HSCB promoter reporter assay.** The human mini promoter region of HSCB was amplified with 5' primer 5' AATTCTCGAGATGACTCACCGCGTGAGCCCACCTGGAGCC 3' and 3' primer 5' AATTAAGCTTAGCAAAGAGAGCGTCTAACCAGACTAATGTTG 3'. The PCR product was digested with XhoI and HindIII and ligated into pGL3 Basic plasmid. The reporter plasmid with G>A SNP was generated by mutagenesis with primers 1) 5' TAGTTTAGAAGGGAGAGCAGAACTTAGAACCCGGGT 3' and 2) 5' ACCCGGGTTCTAAGTTCTGCTCTCCCTTCTAAACTA 3' using the QuikChange kit (Agilent). K562 cells were transfected with 9 µg of control plasmid (pGL3 Basic), wild type reporter plasmid and reporter plasmid with G>A SNP, together with 1 µg of renilla luciferase plasmid (pRL-TK) with the Nucleofector kit (Lonza) according to manufacturer's protocol. The transfected cells were incubated for 48 hrs and the reporter activity was measured using Dual Luciferase Assay System (Promega). The data were analyzed from three independent experiments.

**Chromatin immunoprecipitation (ChIP) and qPCR.** Chromatin immunoprecipitation was performed using the Pierce Agarose ChIP Kit (Thermo Scientific) according to the manufacturer's protocol with slight modifications. Briefly,  $1 \times 10^7$  K562 cells were cross-linked with 1% formaldehyde for 10 minutes at room temperature. 100 µL of prepared nuclei were digested with 6 units of micrococcal nuclease for 15 minutes at 37°C. Immunoprecipitation was completed by incubation of the digested chromatin with 2 µg of control IgG or ETS-1 antibody (Santa Cruz Biotechnology) overnight at 4°C. The IP products were eluted, and DNA was purified with a DNA

clean-up column (Qiagen) according to the manufacturer's protocol. Precipitated DNA encoding the HSCB promoter region was quantified by qPCR with iQ™ SYBR®Green Supermix (Bio-Rad, using the following primers: 5'-CCCTGCCGCCGGACCAATGAGGAGCAGC-3' and 5'-GCAAAGAGAGCGTCTAACCAGACTAATGTTG-3'

**Functional metabolic profiling.** Briefly, experiments were conducted on shRNA-non-infected and shRNA-infected K562 cells on day 6 or 7 on a Seahorse XFe96 extracellular flux analyzer. Seahorse XF Cell "Energy Phenotype" and "Mito Stress Test" kits were used according to the supplier's recommendation (Agilent). K562 cells were counted, and loaded onto a Cell-Tak (Corning, 1206D69) pretreated 96-well cell culture microplate on the day of assay following manufacturer's instructions. An optimal cell density of  $7.5 \times 10^4$  cells per well, FCCP concentration of 0.25  $\mu\text{M}$ , and oligomycin concentration of 1.0  $\mu\text{M}$  was determined empirically. At a minimum, triplicates were performed for each sample on each plate, and three replicate experiments were conducted on different days. Oxygen consumption rate (OCR) and extracellular acidification rates (ECAR) rates were quantified with Seahorse Wave software.

**Flow cytometry.** All washing steps as well as antibody incubations were performed in U bottom plates at 4°C in a sterile PBS supplemented with 2% FBS. Unstained cells were used as negative controls, and single color-stained were employed to set compensation thresholds. BD FACVerse analyzer was used to acquire and analyze the data. Each analysis was conducted at least 3 times on independent samples. Human CD71-FITC antibody (Miltenyi 130-098-781) was used to determine cell surface expression of transferrin receptor 1. Ter119-FITC/CD44-APC (Biolegend 116206/BD Biosciences 559250) staining was used to assess mouse erythroblast maturation using a strategy described by others (13). Lineage-APC (BD Biosciences 51-9003632), Ly-6A/E-PE-Cy7 (Sca-1, Invitrogen 255981-82) and CD117-PE (c-Kit, Ebiosciences 12-1172-83) antibodies were used to identify hematopoietic stem cell (LSK: lineage negative, Sca-1 positive, c-Kit positive). For mouse experiments, bone marrow and spleen were harvested as described

below and filtered with 70  $\mu$ M cell strainers. Prior to LSK staining, red blood cells were lysed using RBC lysis buffer (Qiagen) for 5 minutes at RT.

**Zebrafish.** Zebrafish were maintained and manipulated according to standard procedures(21, 22). AB, *dino* (*din<sup>tm84</sup>*) (23), and a *Tg(globin-LCR:eGFP)* transgenic line (24) were used in this study. The *Tg(globin-LCR:eGFP)* line expresses a GFP reporter under the control of the locus control region (LCR) enhancer of a zebrafish globin gene (24).

*Zebrafish in situ hybridization.* Digoxigenin-labeled cRNA probes were synthesized using DIG RNA labeling kit (Roche). Whole mount *in situ* hybridization (WISH) was carried out as previously described (25). Heterozygous *dino* zebrafish were mated with each other to produce a pool of wild-type and homozygous mutant embryos for WISH analysis.

*Morpholino injections.* Two splice-blocking anti-sense morpholinos for *hscb* were obtained from Gene Tools. The morpholino sequences are 5'-CACAAATACAGTCCATTTACCTGTGA-3' for MO1 and 5'-CTTCGCTGAGGAAAGACAAACACAT-3' for MO2. They are complementary to the exon 2 - intron 2 and intron 1 - exon 2 boundaries of *hscb* pre-mRNA, respectively. The standard control MO from Gene Tools (5'-CCTCTTACCTCAGTTACAATTTATA-3') was used as a negative control. The morpholinos were injected into one-cell stage zebrafish embryos at concentrations of 0.5 mM (MO1 and control MO) and 0.1 mM (MO2). The knockdown efficiency was confirmed by qRT-PCR using primers: *hscb*, 5'-CAGCACAGTTACAGTCAACA-3' and 5'-GGAGAACTCTTTGCAGCTTCAC-3'; *hprt*, 5'-CAGTTAGCTTGTCAGAGTTGGACG-3' and 5'-GTCCACCCATGCCTTTCATTG-3'; *tfr1a*, 5'-AATCGCATTATGAGGGTGGAA-3' and 5'-GGGAGACACGTATGGAGAGAGC-3'

*o-dianisidine staining and quantification of erythrocytes.* Following MO injections, the morphant embryos were harvested at 48~72 hrs post fertilization (hpf) for *o*-dianisidine staining, following the method described previously (26). The morphant embryos from the *Tg(globin-LCR:eGFP)* line were also harvested at 72 hpf for quantification of erythrocytes by fluorescence-activated cell

sorting (FACS). The cells were disaggregated and sequentially filtered through 70  $\mu\text{m}$  and 40  $\mu\text{m}$  cell strainers. The percentage of GFP-positive erythroid cells was analyzed by FACS using the FACSVantage SE machine (BD Biosciences).

*Overexpression of alas2 in zebrafish embryos.* The constructs of *alas2* with IRE in the 5' UTR, *alas2* with 5' IRE (CAGUGC) deleted (-IRE), and the IRE-deleted *alas2* with an engineered premature stop codon (-IRE/\*) at amino acid residue 26 (Tyr26X) were described previously (11, 27). RNAs correlating to these *alas2* variants were synthesized using SP6 mMessage mMachine (Ambion). The RNA (150 ng/ $\mu\text{l}$ ) was injected into one-cell stage zebrafish embryos together with *hscb* MO1 (0.5 mM). At 72 hpf, the morphant embryos were harvested for quantification of erythrocytes by FACS analysis.

*Statistics.* All data are presented as mean  $\pm$  standard error of the mean (SEM). Statistical significance was tested using Paired *t*-test (Panel B) or one-way ANOVA followed by the Tukey-Kramer Multiple Comparisons Test in GraphPad INSTAT version 3.01. A *P* value of  $< 0.05$  was considered as statistically significant.

**Hscb-deficient mice.** Mice heterozygous for an *Hscb* conditional allele (*Hscb<sup>fl/+</sup>*) were derived from conditionally targeted mouse ES cells obtained from the Knockout Mouse Project (KOMP) Consortium. A constitutive null allele (*Hscb<sup>+/-</sup>*) was obtained by breeding the conditional allele to the B6.Cg-Tg(CMV-cre)1Cgn/J line. Both alleles were backcrossed to C57BL/6J for greater than 10 generations each. Dissection of timed matings showed that *Hscb<sup>-/-</sup>* animals die before embryonic day 7.5 (E7.5, data not shown). *Hscb<sup>+/-</sup>* animals were bred individually to the hematopoietic-specific B6.Cg-Tg(Vav1-cre)1Graf (*Vav1-Cre*), the erythroid-specific *Epor<sup>tm1(EGFP/cre)Uk</sup>* (*EpoR-Cre*) and the temporally inducible B6.Cg-Tg(Mx1-Cre)1Cgn/J (*Mx1-Cre*) Cre recombinase lines which were subsequently bred to animals homozygous for the conditional allele (*Hscb<sup>fl/fl</sup>*). All mouse genotypes were determined using the Transnetyx automated genotyping platform.

Fetal liver stem cell transplants using *Hscb*<sup>fl/-</sup> ± *Mx1-Cre* donors were performed as previously described.(28) After 8 weeks, the animals underwent induction of *Mx1-Cre* with poly-inosine-poly-cytosine (pIpC). Each animal received 300 µg of pIpC on alternate days for five days, totaling three injections. Retro-orbital blood was collected for CBCs on days 0, 7, 14, and 22 and diluted 1:4 in PBS for CBCs. Tail nicks were performed to generate blood smears on days 4, 5, 6, 8, 9, 10, and 12 to monitor for the presence of siderocytes in circulation. Complete blood counts (CBCs) were performed on 37.5 µL of blood obtained from a neck vein from 7-day old *Hscb Vav1-Cre* pups and diluted 1:8 in PBS.

**Histology.** P7 pups were fixed whole in 10% buffered formalin for two weeks and embedded in paraffin. Deparaffinized sections of tissue were stained with hematoxylin and eosin, Perls' Prussian blue iron stain or CD71 antibody (Tfr1) in the Boston Children's Hospital, Department of Pathology Histology Laboratory. Images were acquired using either a 10x/0.30 or 4x/0.13 objective lens on a BX51 microscope equipped with a DP71 Digital Camera employing Olympus MicroSuite™ FIVE Imaging Software. May-Grunwald-Giemsa–stained (Sigma-Aldrich) peripheral blood smears were photographed using a 100x/1.3 objective lens.

**Statistical analyses.** All statistical analyses and graphical representations were performed using Graph Pad Prism (version 7.03). One-way ANOVA was performed with multiple comparisons and the uncorrected Fisher's LSD test unless otherwise specified. P<0.05 considered statistically significant. Error bars represent mean ± S.D.

## **Author contributions**

JB, SSB, MMH, DRC, and MDF ascertained and phenotyped patients, processed patient samples and maintained the clinical research database. DRC and AKS performed and interpreted gene/exome sequencing experiments. AC and SD performed fibroblast experiments. CG performed *HSCB* promoter reporter and CHIP experiments in HeLa cells. SD performed K562 Crispr-CAS9 *HSCB* promoter editing and analyses. SD designed and performed most of the shRNA K562 cell studies. AC performed seahorse experiments. AC, DRC, PJS, DL and CCa derived or maintained the *Hscb* null mice. AC, DRC and DS phenotyped the mice. DRC and MDF performed bone marrow transplantations. DS directly supervised AC and DL. CCh, GJHS, NCH, and BHP designed, performed or oversaw zebrafish experiments. MDF and SD reviewed and interpreted all the data. AC, MDF, and SD wrote the manuscript. PJS edited the manuscript. All authors reviewed the final manuscript except BHP; BHP died on December 28, 2017 prior to the completion of the manuscript. The work was presented with his consent during the 59<sup>th</sup> ASH Annual Meeting and Exposition (2017).

## **Acknowledgments**

The authors wish to acknowledge the participation of the index patient and her family as well as all of the congenital sideroblastic anemia patients participating in our research. Ronald Mathieu from the Boston Children's Hospital Division of Hematology/Oncology Harvard Stem Cell Institute provided expert flow cytometry support. Mouse transgenic services were provided by the Boston Children's Hospital Center for Developmental Hematopoiesis Mouse Embryonic Stem Cell and Gene Targeting Core, an NIDDK Cooperative Center of Excellence in Hematology. Nancy Chamberlin is acknowledged for critical review of the manuscript.

## **Funding**

This work was supported by the NIDDK (R01 DK087992, R24 DK094746) and an American Society of Hematology Bridge Grant.

Age (years)	WBC (x10 <sup>3</sup> /μL) [4.5-13.5]	ABS NEUT (x10 <sup>3</sup> /μL) [1.80-7.97]	RBC (x10 <sup>6</sup> /μL) [3.80-5.00]	HGB (g/dL) [12.0-16.0]	HCT (%) [37.0-45.0]	MCV (fl) [78.0-102.0]	MCH (pg) [26.0-32.0]	MCHC (g/dL) [31.0-37.0]	RDW (%) [11.5-14.5]	PLT (x10 <sup>3</sup> /μL) [150-450]	Retic (x10 <sup>6</sup> /μL) [0.043-0.085]	Transfusion status	Marrow RS
9.7	3.72	1.97	4.17	10.4	32.7	78.4	24.8	31.7	24.2	380	0.071	No	NP
12.4	6.77	3.67	3.55	8.9	28.5	80.3	25.1	31.3	23.6	387	0.057	No	NP
13.0*	2.94	1.06	3.35	7.8	26.6	79.2	23.2	29.4	21.9	197	NP	No	NP
14.8	1.83	1.17	1.96	5.5	15.5	79.2	27.9	35.2	12.9	111	NP	8 wks post	NP
15.4	2.25	1.46	2.51	6.7	19.1	76.1	26.8	35.2	13.1	153	NP	8 wks post	Yes
20.3	2.87	1.66	5.36	14.7	41.6	77.6	27.5	35.5	15.4	89	0.025	Chronically	No

**Table 1. Blood counts of the *HSCB-CSA* proband.** WBC, white blood cells; PLT, platelets; HGB, hemoglobin; HCT, hematocrit; RBC, red blood cells; MCV, mean corpuscular volume; MCH, mean corpuscular hemoglobin; MCHC, mean corpuscular hemoglobin concentration; RDW, red cell distribution width; Retic, absolute reticulocytes; RS, ring sideroblasts present on bone marrow aspirate; NP, test was not performed. \*Values at the time of diagnosis of a suprasellar germ cell tumor. Generalized normal ranges are indicated in brackets.

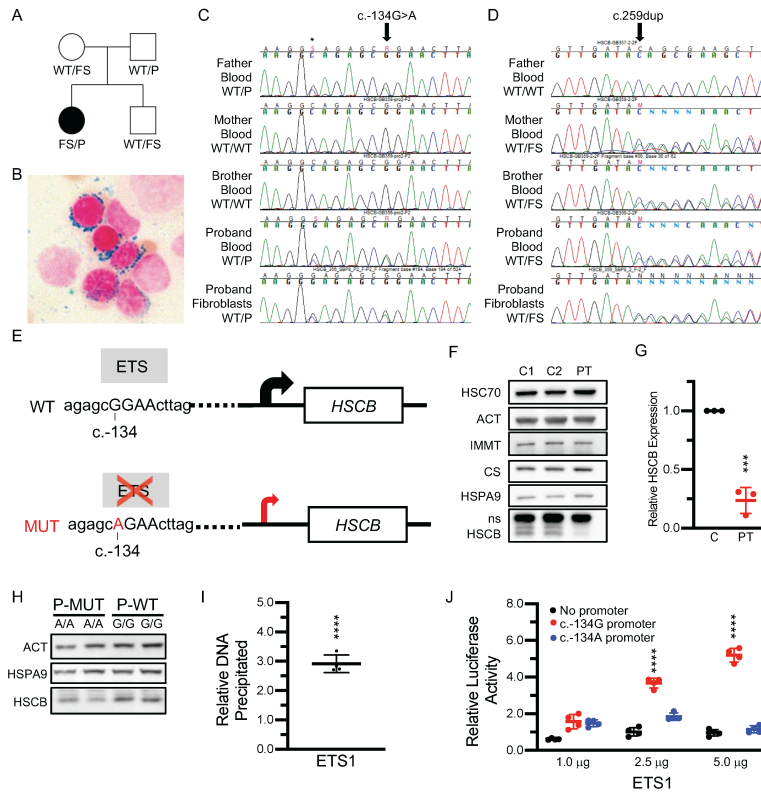


**Figure 1: HSCB expression is decreased by CSA patient-specific mutations.** **A.** Pedigree of the family and *HSCB* variants: wild type (WT) allele, c.-134A>C promoter variant (P), and c.259dup/p.Thr87Asnfs\*27 frameshift allele (FS). **B.** Perls' Prussian blue iron staining of the proband's bone marrow demonstrating characteristic ring sideroblasts. **C. & D.** Sequencing traces of the P and FS variants, respectively. \*indicates a common promoter polymorphism. **E.** Representation of the *HSCB* promoter for the WT or P alleles. Predicted ETS binding site and the consequential reduction in transcription caused by the G/A substitution are indicated by the gray boxes and red arrows, respectively. **F.** Representative western blots of total protein extracts from skin fibroblasts from the proband (PT) and two unrelated female control fibroblast lines (C1 and C2). ACT (actin) and HSC70 (Heat Shock Protein Family 70 member) were used as total protein controls, whereas IMMT (mitofilin) and CS (citrate synthase) control for mitochondrial content. **G.** Quantification of PT and Control (C) fibroblast *HSCB* expression. N=3 Unpaired t test \*\*\*P<0.001. **H.** Western blot of CRISPR/CAS9 edited K562 clones homozygous for the WT (G/G) or the P allele (P-MUT A/A). **I.** Chromatin immunoprecipitation (ChIP) analysis of the *HSCB* promoter region in K562 cells using an ETS1-specific antibody demonstrating specific binding of ETS1 to the c.-134A region. Unpaired t test \*\*\*\*P<0.0001 vs. IgG alone. **J.** Luciferase promoter activity in HeLa cells transfected with a promoterless luciferase expression construct or a similar plasmid containing the *HSCB* promoter with either the WT (c.-134G) or P (c.-134A) variants. Data are normalized to the activity of the promoterless construct co-transfected with 5  $\mu$ g of the ETS1 plasmid. ANOVA \*\*\*\*P<0.0001 vs. no promoter.

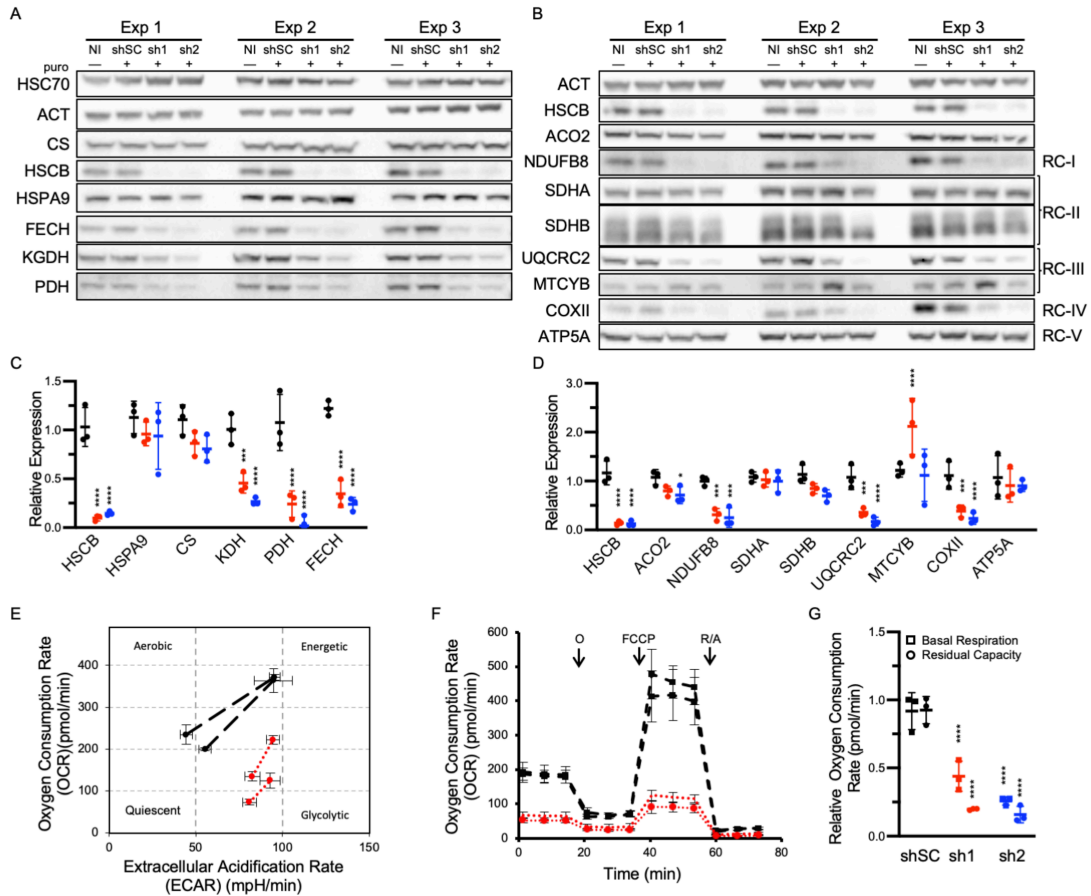
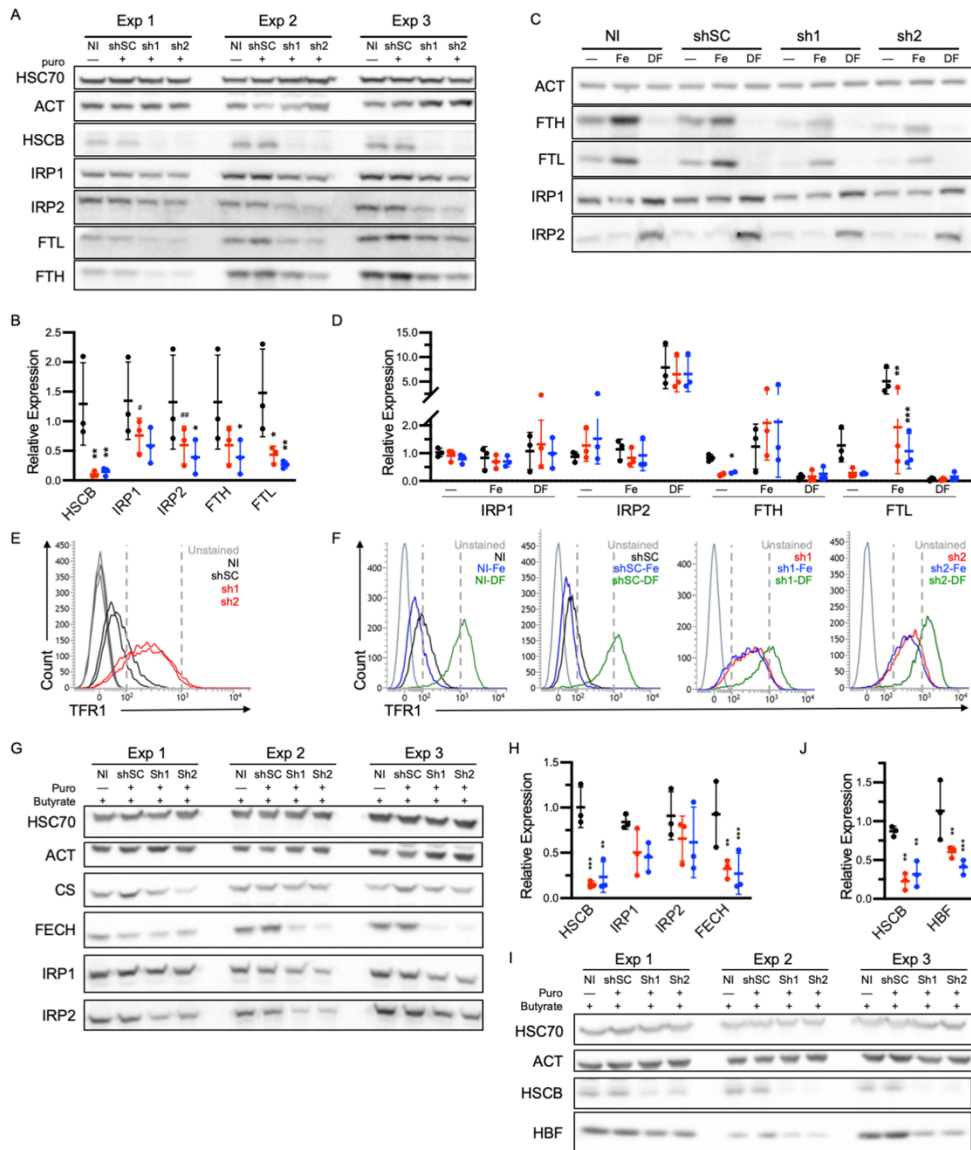


**Figure 2. HSCB depletion decreases Fe-S protein expression and impairs respiration. A. & B.** Western blots of Fe-S biogenesis, Fe-S, and lipoylated proteins (A) and respiratory proteins (B) in K562 erythroleukemia cells 10 days after control and *HSCB*-specific shRNA infection. Three independent experiments are shown. Scrambled control (shSC) and *HSCB*-specific shRNAs 1 (sh1) and 2 (sh2) are colored black, red, and blue, respectively. Uninfected cells are abbreviated NI. **C. & D.** Quantification of western blots in A. & B., respectively. For all panels mean expression  $\pm$  S.D. is normalized to NI cells. ANOVA \* $P < 0.05$ , \*\* $P < 0.01$ , \*\*\* $P < 0.001$  vs. shSC. **E.-G.** Seahorse Extracellular Flux (XF) Analyzer Cell Energy Phenotype analyses of shRNA-treated K562 cells. Data presented are representative of at least three independent experiments. NI and shSC treated K562 cells are indicated in black points with long and short dashes, respectively. sh1 and sh2 treated K562 cells are colored in red and blue, respectively. **E.** Cell Mito Stress Test energy maps of basal (left points) and stressed (right points) oxygen consumption versus extracellular acidification, which is a measure of glycolysis. **F.** Seahorse extracellular flux analysis. Oligomycin (O), carbonyl cyanide *p*-trifluoromethoxy-phenylhydrazone (FCCP), and Rotenone/Antimycin A (R/A) allow assessment of basal ATP production, maximal respiration, and non-mitochondrial respiration, respectively. **G.** Basal respiration and residual respiratory capacity. Activity normalized to NI cells. ANOVA \*\*\*\* $P < 0.001$  vs. shSC. ACO2, aconitase 2; ATP5A, ATP synthase F1 subunit alpha; CS, citrate synthase; COXII, mitochondrially encoded cytochrome C oxidase II; FECH, ferrochelatase; HSPA9, heat shock protein family A (Hsp70) member 9; E2 subunits of pyruvate dehydrogenase (PDH) and  $\alpha$ -ketoglutarate dehydrogenase (KGDH) are detected with an anti-lipoic acid antibody; MTCYB, mitochondrially encoded cytochrome B; NDUFB8, NADH:ubiquinone oxidoreductase subunit B8; OXPHOS, oxidative phosphorylation; RC, respiratory complex; SC, scrambled; SDHB succinate dehydrogenase B subunit; UQCRC2, ubiquinol-cytochrome C reductase core protein 2.



**Figure**

**3. HSCB deficiency affects iron metabolism and hemoglobinization in K562 cells.** **A.** Western blots of 3 independent experiments of iron metabolism proteins in *uninduced* K562 cells infected with viruses encoding scrambled (shSC) and *HSCB*-specific shRNAs (sh1 and sh2) for 10 days. **B.** Quantification of western blots in A. shSC, sh1, and sh2 are colored black, red, and blue, respectively. **C.** Western blots and **D.** quantification of iron metabolism proteins in uninduced K562 cells treated with shRNAs as in A and either iron (Fe) or the iron chelator desferrioxamine (DF) demonstrating reduced expression but retained response of iron regulated proteins to iron concentrations. One representative blot of three independent experiments is shown. Two FTH outliers are removed based on Grubbs test  $p < 0.05$ . **E.** & **F.** TFR1 cell surface expression by flow cytometry of cells in A and C, respectively. **G.-J.** K562 cells treated with shRNAs as in A and differentiated by exposure to sodium butyrate for 96 hrs. Western blotting demonstrating alterations in iron metabolism proteins (**G.** & **H.**) and impaired hemoglobin F expression (**I.** & **J.**). Three independent experiments are shown. For all panels, mean expression  $\pm$  S.D. is normalized to non-infected (NI) cells. ANOVA \* $P < 0.05$ , \*\* $P < 0.01$ , # $P = 0.06$ , ## $P = 0.07$  vs. shSC. IRP, iron regulatory protein; TFR1: transferrin receptor 1.

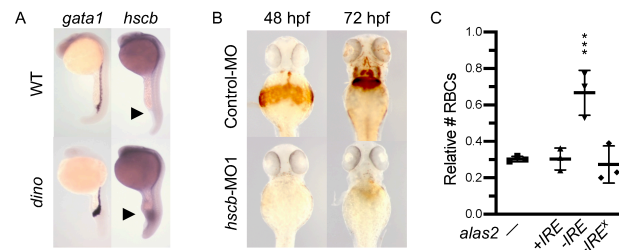


**Figure 4. HSCB depletion in zebrafish embryos impairs hemoglobinization. A.** Whole mount *in situ* hybridization detects ubiquitous expression of *hscb* in zebrafish embryos. *hscb* is weakly expressed in blood islands (arrowheads) at 24 hours post fertilization. The signal in the ventral tissues is enhanced in the embryos from the *dino* mutant, which has a ventralized phenotype (29). *gata1* is an erythroid transcription factor used to mark the blood islands. **B.** *hscb* morpholino (MO1) induces anemia in zebrafish embryos. Reduced o-diansidine (heme) staining is observed at both 48 hpf and 72 hpf in the morphant embryos. **C.** *IRE*-independent expression of *alas2* rescues the erythroid phenotype in *hscb* morphant embryos. *Tg(globin-LCR:eGFP)* transgenic zebrafish embryos were injected with a control morpholino, *hscb*-MO1 (—), *hscb*-MO1 + *alas2* RNA with the 5' IRE (+*IRE*), *hscb*-MO1 + *alas2* RNA without 5' IRE (-*IRE*), and *hscb*-MO1 + *alas2* RNA without 5' IRE but a premature stop codon (-*IRE*<sup>X</sup>). The effect of the *hscb*-MO1 alone and in combination with *alas2* RNAs on the numbers of RBCs per embryo were quantified by flow cytometry. All data are normalized to embryos injected with the control morpholino alone. Data are expressed as mean ±S.D. of 3 independent experiments. ANOVA \*\*P<0.01 vs. *hscb*-MO1 only.

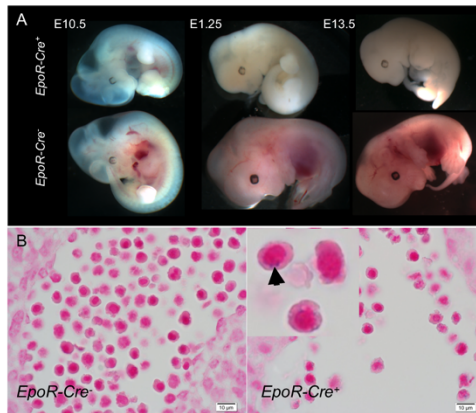


**Figure 5. Prenatal lethality in mice lacking erythroid *Hscb*.** **A.** Erythroid-specific deletion of *Hscb* with *Epor-Cre* results in death due to anemia in embryos before E14.5. Prior to E11.5, when the *Epor-Cre* becomes active, mutant embryos are somewhat hemoglobinized, whereas later embryos show extreme pallor. **B.** Iron-stained histologic sections of E11.5 *Hscb<sup>fl/-</sup> Epor-Cre<sup>+</sup>* animals demonstrate nucleated primitive RBCs containing coarse iron positive granules, consistent with ring sideroblasts. 400x original magnification. Inset 2000x original magnification.

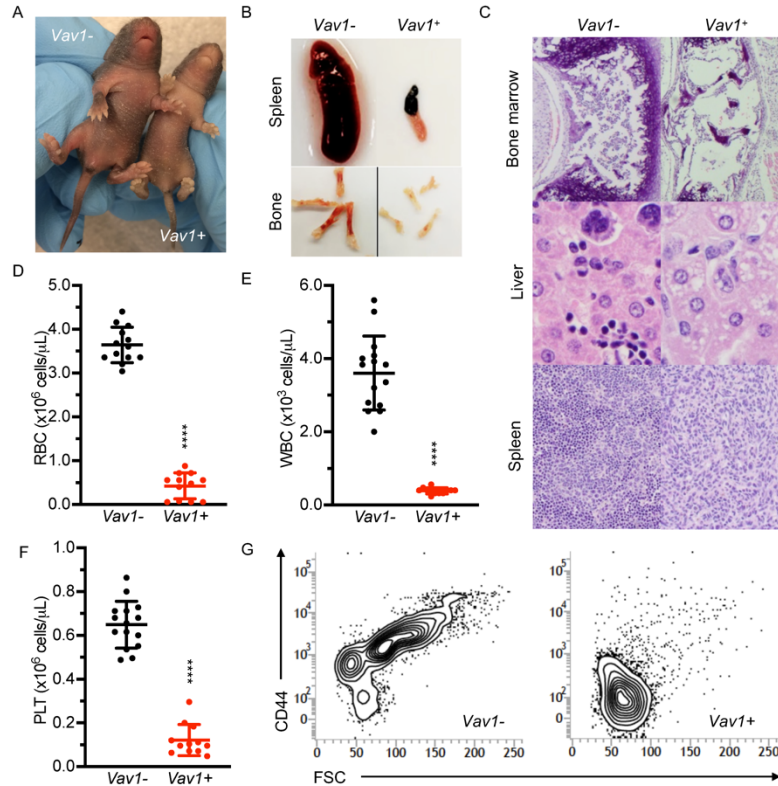


**Figure 6. Post-natal pancytopenia in mice with pan-hematopoietic loss of *Hscb*.** **A.** Post-natal day 7 (P7) *Hscb*<sup>fl/-</sup>±*Vav1*-*Cre*<sup>+</sup> littermates. Control pup (left) and runted, pale *Vav1*-*Cre*<sup>+</sup> (right). **B.** Anemia and lack of erythropoiesis is grossly appreciated by pallor of the long bones in the *Hscb*<sup>fl/-</sup> *Vav1*-*Cre*<sup>+</sup> mutants. The spleens also profoundly atrophic, reflecting a loss of all hematopoietic elements, including lymphocytes. **C.** H&E stained tissue sections of P7 *Hscb*<sup>fl/-</sup> *Vav1*-*Cre*<sup>+</sup> mutant bone marrow (100x original magnification), liver (400x original magnification), and spleen (100x original magnification) show an extreme loss of hematopoietic elements. **D-F.** Profound pancytopenia in P7 *Hscb*<sup>fl/-</sup> *Vav1*-*Cre*<sup>+</sup> animals. In the mutants, hemoglobin (**D**), white blood cell count (**E**), and platelet count (**F**). t test \*\*\*\*P<0.0001. **G.** Representative flow cytometry scattergrams of bone marrow gated on Ter119<sup>+</sup> cells, shows an absence of CD44<sup>+</sup> cells with higher forward scatter (FSC) typical of maturing erythroblasts in the *Hscb*<sup>fl/-</sup>±*Vav1*-*Cre*<sup>+</sup> animals (n=3 in each group).

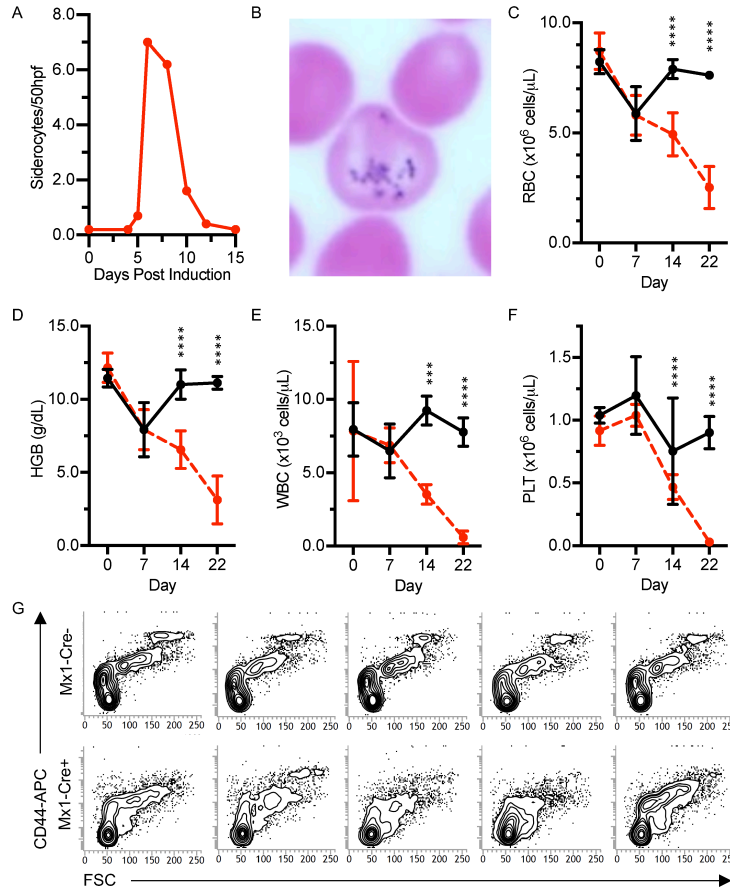


**Figure 7. Hematopoietic deletion of *Hscb* in the adult mouse results in a transient siderocytic anemia and bone marrow failure due to progenitor cell depletion. A.-E.** Time course of cytopenias following *Mx1-Cre*-induced *Hscb* deletion in hematopoietic stem cell transplant chimeras. Adult animals were transplanted with *Hscb*<sup>fl/-</sup>±*Mx1-Cre* fetal liver cells and allowed to engraft for 8 weeks. Thereafter, *Hscb* deletion was induced by injection with poly-inosine, poly-cytosine (plpC). **A-B.** There is a transient population of siderocytes present only in the *Mx1-Cre*<sup>+</sup> animals that peaks on day 7 after the initiation of induction. Beginning after day 7 of induction, *Mx1-Cre*<sup>+</sup> animals experience a precipitous drop in (**C**) red blood cells (RBC), (**D**) hemoglobin (HGB), (**E**) white blood cells (WBC), and (**F**) platelets (PLT). n=5 in each group. Decreases in RBC, HGB, and WBC and an increase in PLT, observed immediately after induction (day 7), are likely related to plpC-induced cytokines. ANOVA \*\*\*P<0.001, \*\*\*\*P<0.0001. **G.** Flow cytometry scattergrams of bone marrow gated on Ter119<sup>+</sup> cells, shows a decrease in CD44<sup>+</sup> cells with higher forward scatter (FSC) typical of maturing erythroblasts in the *Hscb*<sup>fl/-</sup>± *MX1-Cre*<sup>+</sup> animals (n=5 in each group).

## References

1. Ducamp S, and Fleming MD. The molecular genetics of sideroblastic anemia. *Blood*. 2019;133(1):59-69.
2. Rouault TA, and Maio N. Biogenesis and functions of mammalian iron-sulfur proteins in the regulation of iron homeostasis and pivotal metabolic pathways. *J Biol Chem*. 2017;292(31):12744-53.
3. Braymer JJ, and Lill R. Iron-sulfur cluster biogenesis and trafficking in mitochondria. *J Biol Chem*. 2017;292(31):12754-63.
4. Crooks DR, Ghosh MC, Haller RG, Tong WH, and Rouault TA. Posttranslational stability of the heme biosynthetic enzyme ferrochelatase is dependent on iron availability and intact iron-sulfur cluster assembly machinery. *Blood*. 2010;115(4):860-9.
5. Wang H, Shi H, Rajan M, Canarie ER, Hong S, Simoneschi D, et al. FBXL5 Regulates IRP2 Stability in Iron Homeostasis via an Oxygen-Responsive [2Fe2S] Cluster. *Mol Cell*. 2020;78(1):31-41 e5.
6. Findlay VJ, LaRue AC, Turner DP, Watson PM, and Watson DK. Understanding the role of ETS-mediated gene regulation in complex biological processes. *Adv Cancer Res*. 2013;119:1-61.
7. Kim KS, Maio N, Singh A, and Rouault TA. Cytosolic HSC20 integrates de novo iron-sulfur cluster biogenesis with the CIAO1-mediated transfer to recipients. *Hum Mol Genet*. 2018;27(5):837-52.
8. Maio N, Kim KS, Singh A, and Rouault TA. A Single Adaptable Cochaperone-Scaffold Complex Delivers Nascent Iron-Sulfur Clusters to Mammalian Respiratory Chain Complexes I-III. *Cell Metab*. 2017;25(4):945-53 e6.
9. Uhrigshardt H, Singh A, Kovtunovych G, Ghosh M, and Rouault TA. Characterization of the human HSC20, an unusual DnaJ type III protein, involved in iron-sulfur cluster biogenesis. *Hum Mol Genet*. 2010;19(19):3816-34.
10. Ollagnier-De Choudens S, Sanakis Y, Hewitson KS, Roach P, Baldwin JE, Munck E, et al. Iron-sulfur center of biotin synthase and lipoate synthase. *Biochemistry*. 2000;39(14):4165-73.
11. Wingert RA, Galloway JL, Barut B, Foott H, Fraenkel P, Axe JL, et al. Deficiency of glutaredoxin 5 reveals Fe-S clusters are required for vertebrate haem synthesis. *Nature*. 2005;436(7053):1035-39.
12. Heinrich AC, Pelanda R, and Klingmuller U. A mouse model for visualization and conditional mutations in the erythroid lineage. *Blood*. 2004;104(3):659-66.
13. Liu J, Zhang J, Ginzburg Y, Li H, Xue F, De Franceschi L, et al. Quantitative analysis of murine terminal erythroid differentiation in vivo: novel method to study normal and disordered erythropoiesis. *Blood*. 2013;121(8):e43-9.
14. Voisine C, Cheng YC, Ohlson M, Schilke B, Hoff K, Beinert H, et al. Jac1, a mitochondrial J-type chaperone, is involved in the biogenesis of Fe/S clusters in *Saccharomyces cerevisiae*. *Proceedings of the National Academy of Sciences of the United States of America*. 2001;98(4):1483-8.
15. Schmitz-Abe K, Ciesielski SJ, Schmidt PJ, Campagna DR, Rahimov F, Schilke BA, et al. Congenital sideroblastic anemia due to mutations in the mitochondrial HSP70 homologue HSPA9. *Blood*. 2015;126(25):2734-8.
16. Ye H, Jeong SY, Ghosh MC, Kovtunovych G, Silvestri L, Ortillo D, et al. Glutaredoxin 5 deficiency causes sideroblastic anemia by specifically impairing heme biosynthesis and depleting cytosolic iron in human erythroblasts. *J Clin Invest*. 2010;120(5):1749-61.
17. Rademakers LH, Koningsberger JC, Sorber CW, Baart de la Faille H, Van Hattum J, and Marx JJ. Accumulation of iron in erythroblasts of patients with erythropoietic protoporphyria. *Eur J Clin Invest*. 1993;23(2):130-8.

18. Tanimura N, Miller E, Igarashi K, Yang D, Burstyn JN, Dewey CN, et al. Mechanism governing heme synthesis reveals a GATA factor/heme circuit that controls differentiation. *EMBO Rep.* 2016;17(2):249-65.
19. Doty RT, Yan X, Lausted C, Munday AD, Yang Z, Yi D, et al. Single-cell analyses demonstrate that a heme-GATA1 feedback loop regulates red cell differentiation. *Blood.* 2019;133(5):457-69.
20. Ran FA, Hsu PD, Wright J, Agarwala V, Scott DA, and Zhang F. Genome engineering using the CRISPR-Cas9 system. *Nat Protoc.* 2013;8(11):2281-308.
21. Lawrence C, Adatto I, Best J, James A, and Maloney K. Generation time of zebrafish (*Danio rerio*) and medakas (*Oryzias latipes*) housed in the same aquaculture facility. *Lab animal.* 2012;41(6):158-65.
22. Westerfield M. *The zebrafish book. A guide for the laboratory use of zebrafish (Danio rerio)*. Eugene, OR: University of Oregon Press; 2000.
23. Haffter P, Granato M, Brand M, Mullins MC, Hammerschmidt M, Kane DA, et al. The identification of genes with unique and essential functions in the development of the zebrafish, *Danio rerio*. *Development.* 1996;123:1-36.
24. Ganis JJ, Hsia N, Trompouki E, de Jong JL, DiBiase A, Lambert JS, et al. Zebrafish globin switching occurs in two developmental stages and is controlled by the LCR. *Dev Biol.* 2012;366(2):185-94.
25. Chen C, Garcia-Santos D, Ishikawa Y, Seguin A, Li L, Fegan KH, et al. Snx3 regulates recycling of the transferrin receptor and iron assimilation. *Cell Metab.* 2013;17(3):343-52.
26. Shaw GC, Cope JJ, Li L, Corson K, Hersey C, Ackermann GE, et al. Mitoferrin is essential for erythroid iron assimilation. *Nature.* 2006;440(7080):96-100.
27. Chung J, Anderson SA, Gwynn B, Deck KM, Chen MJ, Langer NB, et al. Iron regulatory protein-1 protects against mitoferrin-1-deficient porphyria. *J Biol Chem.* 2014;289(11):7835-43.
28. Ohgami RS, Campagna DR, Antiochos B, Wood EB, Sharp JJ, Barker JE, et al. nm1054: a spontaneous, recessive, hypochromic, microcytic anemia mutation in the mouse. *Blood.* 2005;106(10):3625-31.
29. Hammerschmidt M, Pelegri F, Mullins MC, Kane DA, Brand M, van Eeden FJ, et al. Mutations affecting morphogenesis during gastrulation and tail formation in the zebrafish, *Danio rerio*. *Development.* 1996;123:143-51.